Evidence for direct CP violation in the decay $B^{\pm} \to D^{(*)} K^{\pm}, D \to K^0_S \pi^+ \pi^-$ and measurement of the CKM phase ϕ_3

A. Poluektov,[1,34] A. Bondar,[1,34] B. D. Yabsley,[41] I. Adachi,[9] H. Aihara,[47] K. Arinstein,[1,34] V. Aulchenko,[1,34] T. Aushev,[20,13] A. M. Bakich,[41] V. Balagura,[13] E. Barberio,[24] A. Bay,[20] K. Belous,[12] M. Bischofberger,[26] A. Bozek,[30] M. Bračko,[22,14] T. E. Browder,[8] M.-C. Chang,[4] P. Chang,[29] A. Chen,[27] K.-F. Chen,[29] P. Chen,[29] B. G. Cheon,[7] I.-S. Cho,[51] Y. Choi,[40] J. Dalseno,[23,43] M. Danilov,[13] M. Dash,[50] A. Drutskoy,[3] W. Dungel,[11] S. Eidelman,[1,34] D. Epifanov,[1,34] N. Gabyshev,[1,34] A. Garmash,[1,34] P. Goldenzweig,[3] B. Golob,[21,14] H. Ha,[18] J. Haba,[9] H. Hayashii,[26] Y. Horii,[46] Y. Hoshi,[45] W.-S. Hou,[29] Y. B. Hsiung,[29] H. J. Hyun,[19] T. Iijima,[25] K. Inami,[25] M. Iwabuchi,[51] M. Iwasaki,[47] Y. Iwasaki,[9] N. J. Joshi,[42] T. Julius,[24] D. H. Kah,[19] J. H. Kang,[51] P. Kapusta,[30] N. Katayama,[9] T. Kawasaki,[32] C. Kiesling,[23] H. J. Kim,[19] H. O. Kim,[19] J. H. Kim,[17] M. J. Kim,[19] Y. J. Kim,[6] K. Kinoshita,[3] B. R. Ko,[18] P. Kodyš,[2] S. Korpar,[22,14] P. Križan,[21,14] P. Krokovny,[9] T. Kuhr,[16] R. Kumar,[35] A. Kuzmin,[1,34] Y.-J. Kwon,[51] S.-H. Kyeong,[51] J. S. Lange,[5] M. J. Lee,[39] S.-H. Lee,[18] J. Li,[8] C. Liu,[38] D. Liventsev,[13] R. Louvot,[20] A. Matyja,[30] S. McOnie,[41] K. Miyabayashi,[26] H. Miyata,[32] Y. Miyazaki,[25] R. Mizuk,[13] G. B. Mohanty,[42] M. Nakao,[9] Z. Natkaniec,[30] S. Neubauer,[16] S. Nishida,[9] K. Nishimura,[8] O. Nitoh,[49] S. Ogawa,[44] T. Ohshima,[25] S. Okuno,[15] S. L. Olsen,[39,8] G. Pakhlova,[13] H. K. Park,[19] M. Petrič,[14] L. E. Piilonen,[50] M. Röhrken,[16] S. Ryu,[39] H. Sahoo,[8] Y. Sakai,[9] O. Schneider,[20] C. Schwanda,[11] A. J. Schwartz,[3] K. Senyo,[25] M. E. Sevior,[24] M. Shapkin,[12] V. Shebalin,[1,34] C. P. Shen,[8] J.-G. Shiu,[29] B. Shwartz,[1,34] J. B. Singh,[35] P. Smerkol,[14] A. Sokolov,[12] S. Stanič,[33] M. Starič,[14] K. Sumisawa,[9] T. Sumiyoshi,[48] S. Suzuki,[37] M. Tanaka,[9] K. Trabelsi,[9] T. Tsuboyama,[9] S. Uehara,[9] S. Uno,[9] Y. Usov,[1,34] G. Varner,[8] K. E. Varvell,[41] K. Vervink,[20] A. Vinokurova,[1,34] C. H. Wang,[28] J. Wang,[36] M.-Z. Wang,[29] P. Wang,[10] X. L. Wang,[10] M. Watanabe,[32] Y. Watanabe,[15] R. Wedd,[24] E. Won,[18] H. Yamamoto,[46] Y. Yamashita,[31] Z. P. Zhang,[38] V. Zhilich,[1,34] V. Zhulanov,[1,34] T. Zivko,[14] A. Zupanc,[16] and O. Zyukova[1,34]

(Belle Collaboration)

[1]*Budker Institute of Nuclear Physics, Novosibirsk*
[2]*Faculty of Mathematics and Physics, Charles University, Prague*
[3]*University of Cincinnati, Cincinnati, Ohio 45221*
[4]*Department of Physics, Fu Jen Catholic University, Taipei*
[5]*Justus-Liebig-Universität Gießen, Gießen*
[6]*The Graduate University for Advanced Studies, Hayama*
[7]*Hanyang University, Seoul*
[8]*University of Hawaii, Honolulu, Hawaii 96822*
[9]*High Energy Accelerator Research Organization (KEK), Tsukuba*
[10]*Institute of High Energy Physics, Chinese Academy of Sciences, Beijing*
[11]*Institute of High Energy Physics, Vienna*
[12]*Institute of High Energy Physics, Protvino*
[13]*Institute for Theoretical and Experimental Physics, Moscow*
[14]*J. Stefan Institute, Ljubljana*
[15]*Kanagawa University, Yokohama*
[16]*Institut für Experimentelle Kernphysik, Karlsruhe Institut für Technologie, Karlsruhe*
[17]*Korea Institute of Science and Technology Information, Daejeon*
[18]*Korea University, Seoul*
[19]*Kyungpook National University, Taegu*
[20]*École Polytechnique Fédérale de Lausanne (EPFL), Lausanne*
[21]*Faculty of Mathematics and Physics, University of Ljubljana, Ljubljana*
[22]*University of Maribor, Maribor*
[23]*Max-Planck-Institut für Physik, München*
[24]*University of Melbourne, School of Physics, Victoria 3010*
[25]*Nagoya University, Nagoya*
[26]*Nara Women's University, Nara*
[27]*National Central University, Chung-li*
[28]*National United University, Miao Li*
[29]*Department of Physics, National Taiwan University, Taipei*
[30]*H. Niewodniczanski Institute of Nuclear Physics, Krakow*
[31]*Nippon Dental University, Niigata*
[32]*Niigata University, Niigata*

[33]*University of Nova Gorica, Nova Gorica*
[34]*Novosibirsk State University, Novosibirsk*
[35]*Panjab University, Chandigarh*
[36]*Peking University, Beijing*
[37]*Saga University, Saga*
[38]*University of Science and Technology of China, Hefei*
[39]*Seoul National University, Seoul*
[40]*Sungkyunkwan University, Suwon*
[41]*School of Physics, University of Sydney, NSW 2006*
[42]*Tata Institute of Fundamental Research, Mumbai*
[43]*Excellence Cluster Universe, Technische Universität München, Garching*
[44]*Toho University, Funabashi*
[45]*Tohoku Gakuin University, Tagajo*
[46]*Tohoku University, Sendai*
[47]*Department of Physics, University of Tokyo, Tokyo*
[48]*Tokyo Metropolitan University, Tokyo*
[49]*Tokyo University of Agriculture and Technology, Tokyo*
[50]*IPNAS, Virginia Polytechnic Institute and State University, Blacksburg, Virginia 24061*
[51]*Yonsei University, Seoul*

(Received 18 March 2010; published 16 June 2010)

We present a new measurement of the unitarity triangle angle ϕ_3 using a Dalitz plot analysis of the $K^0_S\pi^+\pi^-$ decay of the neutral D meson produced in $B^\pm \to D^{(*)}K^\pm$ decays. The method exploits the interference between D^0 and $\bar{D}^0$ to extract the angle ϕ_3, strong phase δ, and the ratio r of suppressed and allowed amplitudes. We apply this method to a 605 fb^{-1} data sample collected by the Belle experiment. The analysis uses three decays: $B^\pm \to DK^\pm$, and $B^\pm \to D^*K^\pm$ with $D^* \to D\pi^0$ and $D^* \to D\gamma$, as well as the corresponding charge-conjugate modes. From a combined maximum likelihood fit to the three modes, we obtain $\phi_3 = 78.4^\circ\,^{+10.8^\circ}_{-11.6^\circ} \pm 3.6^\circ(\text{syst}) \pm 8.9^\circ(\text{model})$. CP conservation in this process is ruled out at the confidence level $(1 - CL) = 5 \times 10^{-4}$, or 3.5 standard deviations.

DOI: 10.1103/PhysRevD.81.112002 PACS numbers: 12.15.Hh, 13.25.Hw, 14.40.Nd

I. INTRODUCTION

Determinations of parameters of the Cabibbo-Kobayashi-Maskawa (CKM) matrix [1] are important as checks on the consistency of the standard model and as ways to search for new physics. Among the angles of the CKM unitarity triangle, ϕ_3 (also widely known as γ) is the least-well constrained by direct measurements, so new results are of particular interest. The principal experimental resource is CP violation in the family of decays $B \to DK$: various methods for extracting a ϕ_3 measurement have been proposed [2–5], following the original discussion of direct CP violation measurement by Bigi, Carter, and Sanda [6]. The most sensitive technique relies on three-body final states [7,8] such as $K^0_S\pi^+\pi^-$.

In the Wolfenstein parameterization of the CKM matrix elements [9], the weak parts of the amplitudes that contribute to the decay $B^+ \to DK^+$ are given by $V^*_{cb}V_{us} \sim A\lambda^3$ (for the $\bar{D}^0K^+$ final state) and $V^*_{ub}V_{cs} \sim A\lambda^3(\rho + i\eta)$ (for D^0K^+); the two amplitudes interfere as the D^0 and $\bar{D}^0$ mesons decay into the same final state $K^0_S\pi^+\pi^-$. Assuming no CP asymmetry in neutral D decays, the amplitude for the process $B^\pm \to (K^0_S\pi^+\pi^-)_D K^\pm$ as a function of the Dalitz plot variables $m^2_+ = m^2_{K^0_S\pi^+}$ and $m^2_- = m^2_{K^0_S\pi^-}$ is

$$M_\pm = f(m^2_\pm, m^2_\mp) + re^{\pm i\phi_3 + i\delta} f(m^2_\mp, m^2_\pm), \qquad (1)$$

where $f(m^2_+, m^2_-)$ is the amplitude of the $\bar{D}^0 \to K^0_S\pi^+\pi^-$ decay, r is the ratio of the magnitudes of the two interfering amplitudes, and δ is the strong phase difference between them. The $\bar{D}^0 \to K^0_S\pi^+\pi^-$ decay amplitude f can be determined from a large sample of flavor-tagged $\bar{D}^0 \to K^0_S\pi^+\pi^-$ decays produced in continuum e^+e^- annihilation. Once f is known, a simultaneous fit to B^+ and B^- data allows the contributions of r, ϕ_3, and δ to be separated. The method has a twofold ambiguity: (ϕ_3, δ) and $(\phi_3 + 180^\circ, \delta + 180^\circ)$ solutions cannot be separated. We always choose the solution with $0 < \phi_3 < 180^\circ$. We neglect the effects of charm mixing in this formalism. Given the current precision of ϕ_3 and the constraints on the D^0 mixing parameters ($x_D, y_D \sim 0.01$ [10]), these effects can be safely neglected [11], although it is possible to take them into account if they appear to be significant for future precision measurements. References [7,12] give a more detailed description of the technique.

This method can be applied to other decay modes: in addition to $B^+ \to DK^+$,[1] excited states of neutral D and K can also be used, although the values of δ and r can differ

[1]Charge-conjugate modes are implied throughout the paper unless noted otherwise.

for these decays. Both the *BABAR* and Belle Collaborations have successfully applied this technique to $B^\pm \to D^{(*)}K^{(*)\pm}$ modes with D^0 decaying to $K^0_S\pi^+\pi^-$ [12–16]. In addition, the *BABAR* Collaboration reported a measurement of ϕ_3 using the $B^\pm \to DK^\pm$ mode with the D decaying to the $K^0_S K^+ K^-$ [16] and $\pi^0\pi^+\pi^-$ [17] final states.

Here we present a measurement of ϕ_3 using the modes $B^+ \to DK^+$ and $B^+ \to D^*K^+$ with $D \to K^0_S\pi^+\pi^-$, based on a 605 fb^{-1} data sample (657×10^6 $B\bar{B}$ pairs) collected by the Belle detector at the KEKB asymmetric e^+e^- collider. The Belle detector is described in detail elsewhere [18,19]. It is a large-solid-angle magnetic spectrometer consisting of a silicon vertex detector, a 50-layer central drift chamber for charged particle tracking and specific ionization measurement (dE/dx), an array of aerogel threshold Cherenkov counters, time-of-flight scintillation counters, and an array of CsI(Tl) crystals for electromagnetic calorimetry located inside a superconducting solenoid coil that provides a 1.5 T magnetic field. An iron flux return located outside the coil is instrumented to detect K_L mesons and identify muons.

The results presented in this paper supersede our previous measurement based on a sample of 386×10^6 $B\bar{B}$ pairs [12]. In addition to $B^\pm \to DK^\pm$ and the $B^\pm \to D^*K^\pm$ mode with $D^* \to D\pi^0$, this analysis exploits $B^\pm \to D^*K^\pm$ with $D^* \to D\gamma$. The $D^* \to D\gamma$ mode has nearly the same parameters as $B^\pm \to D^*K^\pm$ with $D^* \to D\pi^0$, the only difference being that due to the opposite C parities of the γ and π^0, the strong phases for these modes differ by 180° [20]. This provides an additional cross-check for the analysis and allows systematic uncertainties in the combined measurement to be reduced. The analysis procedure is also improved. It uses additional variables in the maximum likelihood fit for the separation of signal from background; this allows one to relax some selection requirements, thus increasing the sample size.

II. EVENT SELECTION

The decay chains $B^+ \to DK^+$ and $B^+ \to D^*K^+$ with $D^* \to D\pi^0$ and $D^* \to D\gamma$ are selected for the analysis. The neutral D meson is reconstructed in the $K^0_S\pi^+\pi^-$ final state in all cases. We also select decays $D^{*-} \to \bar{D}^0\pi^-$ produced via the $e^+e^- \to c\bar{c}$ continuum process as a high-statistics sample to determine the $\bar{D}^0 \to K^0_S\pi^+\pi^-$ decay amplitude.

Charged tracks are required to satisfy criteria based on the quality of the track fit and the distance from the interaction point. We require each track to have a transverse momentum greater than 100 MeV/c. (The reference axis is given by the direction of the e^+ beam.) Separation of kaons and pions is accomplished by combining the responses of the aerogel threshold Cherenkov counters and the time-of-flight scintillation counters with the dE/dx measurement from the central drift chamber. Photon candidates are required to have an energy measured by the electromagnetic calorimeter greater than 30 MeV. Neutral pion candidates are formed from pairs of photons with invariant masses in the range 120–150 MeV/c^2. Neutral kaons are reconstructed from pairs of oppositely charged tracks with an invariant mass $M_{\pi\pi}$ within 7 MeV/c^2 of the nominal K^0_S mass and forming a vertex more than 1 mm from the interaction point in the transverse plane.

To determine the $\bar{D}^0 \to K^0_S\pi^+\pi^-$ decay amplitude we use $D^{*\pm}$ mesons produced via the $e^+e^- \to c\bar{c}$ continuum process. The flavor of the neutral D meson is tagged by the charge of the slow pion (which we denote as π_s) in the decay $D^{*-} \to \bar{D}^0\pi^-_s$. The slow pion track is fitted to the $\bar{D}^0$ production vertex to improve the momentum and angular resolution of the π_s. To select neutral D candidates we require the invariant mass of the $K^0_S\pi^+\pi^-$ system to be within 11 MeV/c^2 of the D^0 mass. To select events originating from a D^{*-} decay we impose a requirement on the difference ΔM of the invariant masses of the D^{*-} and the neutral D candidates: 144.9 MeV/$c^2 < \Delta M <$ 145.9 MeV/c^2. Suppression of the combinatorial background from $B\bar{B}$ events is achieved by requiring the D^{*-} momentum in the center-of-mass (CM) frame to be greater than 3.0 GeV/c. The number of events in the signal region is 290.9×10^3; the background fraction is 1.0%.

The selection of B candidates is based on the CM energy difference $\Delta E = \sum E_i - E_{\rm beam}$ and the beam-constrained B meson mass $M_{\rm bc} = \sqrt{E^2_{\rm beam} - (\sum \vec{p}_i)^2}$, where $E_{\rm beam}$ is the CM beam energy and E_i and $\vec{p}_i$ are the CM energies and momenta of the B candidate decay products. We select events with $M_{\rm bc} > 5.2$ GeV/c^2 and $|\Delta E| < 0.15$ GeV for further analysis. We also impose a requirement on the invariant mass of the neutral D candidate as above: $|M_{K^0_S\pi^+\pi^-} - M_{D^0}| < 11$ MeV/c^2. To obtain the Dalitz plot variables m^2_+ and m^2_-, a kinematical fit is employed with the constraint that the $K^0_S\pi^+\pi^-$ invariant mass be equal to M_{D^0}.

We consider two major background sources in our data: the continuum process $e^+e^- \to q\bar{q}$, where the light component with $q = u, d, s$ and the charmed component are treated separately; and $B\bar{B}$ decays, where events with real D^0 (due to $B^\pm \to D\pi^\pm$, etc.) are treated separately. To suppress background from continuum events, we calculate two variables that characterize the event shape. One is the cosine of the thrust angle $\cos\theta_{\rm thr}$, where $\theta_{\rm thr}$ is the angle between the thrust axis of the B candidate daughters and that of the rest of the event, calculated in the CM frame. The other is a Fisher discriminant $\mathcal{F}$ composed of 11 parameters [21]: the production angle of the B candidate, the angle of the B thrust axis relative to the beam axis, and nine parameters representing the momentum flow in the event relative to the B thrust axis in the CM frame. In the first stage of the analysis, the $(M_{\rm bc}, \Delta E)$ distribution is fitted in order to obtain the fractions of the background

components, and we require $|\cos\theta_{\rm thr}| < 0.8$ and $\mathcal{F} > -0.7$. In the Dalitz plot fit, we do not reject events based on these variables (as in the previous analysis [12]) but rather use them in the likelihood function to better separate signal and background events. This leads to a 7%–8% improvement in the expected statistical error.

The ΔE and $M_{\rm bc}$ distributions for the $B^+ \to DK^+$ mode are shown in Fig. 1(a) and 1(b). For the selected events a two-dimensional unbinned maximum likelihood fit in the variables $M_{\rm bc}$ and ΔE is performed, with the fractions of continuum, $B\bar{B}$, and $B^\pm \to D^{(*)}\pi^\pm$ backgrounds as free parameters, and their distributions fixed from generic Monte Carlo (MC) simulation. [The continuum component

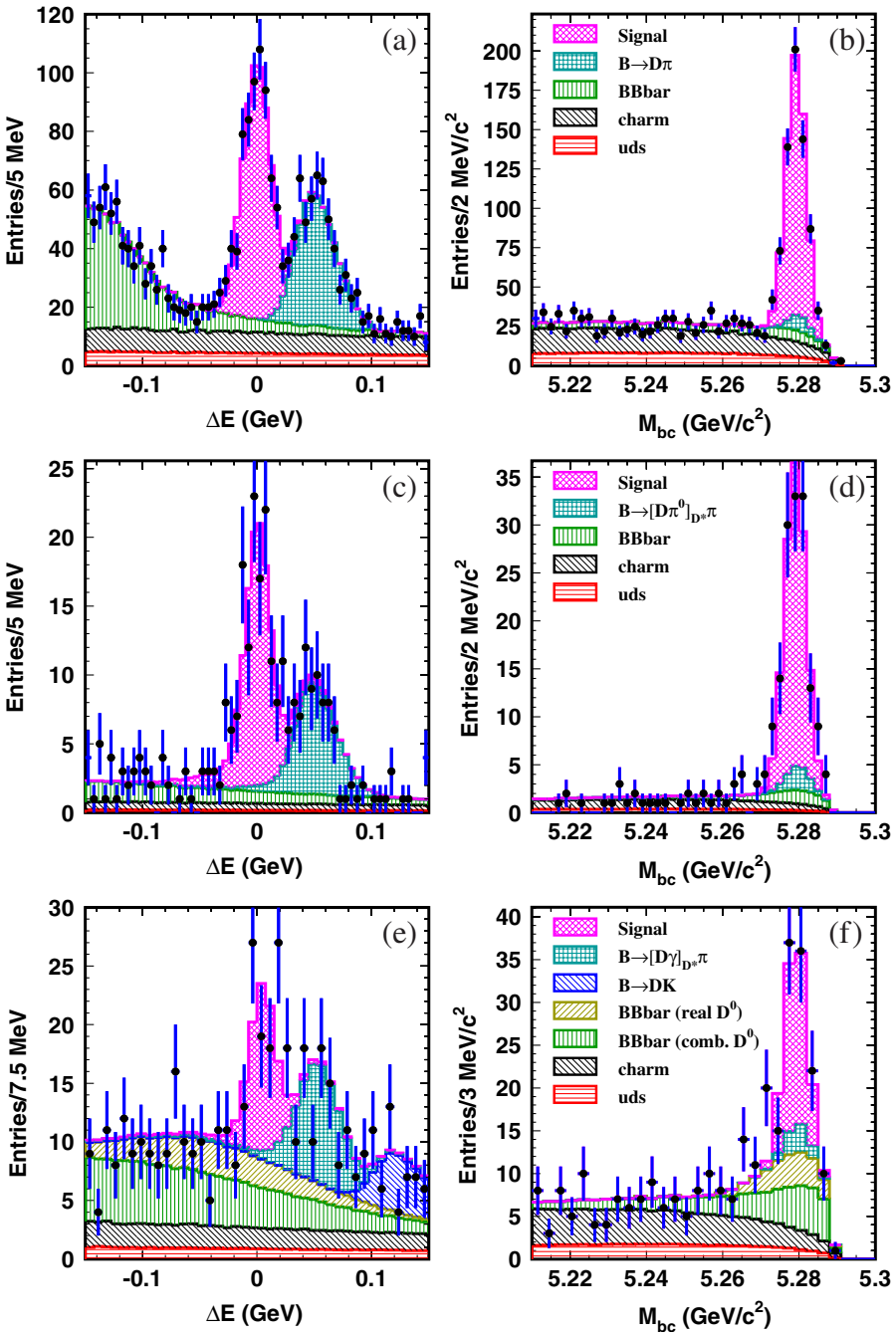

FIG. 1 (color online). ΔE and $M_{\rm bc}$ distributions for the $B^+ \to DK^+$ (a),(b), $B^+ \to D^*K^+$ with $D^* \to D\pi^0$ (c),(d), and $B^+ \to D^*K^+$ with $D^* \to D\gamma$ (e),(f) event samples. Points with error bars are the data, and the histograms are fitted contributions due to signal, misidentified $B^\pm \to D^{(*)}\pi^\pm$ events, and $B\bar{B}$, charm, and (u, d, s) backgrounds; in (e), a $B^\pm \to DK^\pm$ contribution with a random photon is also included. ΔE distributions are plotted with a $M_{\rm bc} > 5.27$ MeV/c^2 requirement; $M_{\rm bc}$ distributions use a $|\Delta E| < 30$ MeV requirement. $|\cos\theta_{\rm thr}| < 0.8$ and $\mathcal{F} > -0.7$ requirements are used in all the plots.

is also split into (u, d, s) and charm components in the figure, based on fractions in the MC.] The resulting signal and background fractions are used in the Dalitz plot fit to obtain the event-by-event signal-to-background ratio. A more detailed description of the two-stage procedure is given in Sec. IV. The number of events in the signal box ($M_{\rm bc} > 5.27$ GeV/c^2, $|\Delta E| < 30$ MeV, $|\cos\theta_{\rm thr}| < 0.8$, $\mathcal{F} > -0.7$) is 756, with a signal purity of $(70.5 \pm 1.2)\%$. The $(M_{\rm bc}, \Delta E)$ fit yields a continuum background fraction of $(17.9 \pm 0.7)\%$, a $B\bar{B}$ background fraction of $(7.3 \pm 0.5)\%$, and a $B^{\pm} \to D\pi^{\pm}$ background fraction of $(4.3 \pm 0.3)\%$ in the signal box. Figure 2 shows the distributions of $\cos\theta_{\rm thr}$ and $\mathcal{F}$ variables in the $M_{\rm bc}$, ΔE signal region for the $B^+ \to DK^+$ mode. The distributions for the other modes are similar.

To select $B^+ \to D^*K^+$ events with $D^* \to D\pi^0$, in addition to the requirements described above, we require that the mass difference ΔM of neutral D^* and D candidates satisfies $140\ {\rm MeV}/c^2 < \Delta M < 144\ {\rm MeV}/c^2$. The ΔE and $M_{\rm bc}$ distributions for this mode are shown in Fig. 1(c) and 1(d). The background fractions are obtained in the same way as for the $B^{\pm} \to DK^{\pm}$ mode. The number of events in the signal box is 149, with $(79.7 \pm 2.5)\%$ signal purity. The continuum background fraction is $(5.7 \pm 0.7)\%$, the $B\bar{B}$ background fraction is $(7.6 \pm 1.9)\%$, and the $B^{\pm} \to D^*\pi^{\pm}$ background fraction is $(7.0 \pm 1.3)\%$.

Selection of the $B^+ \to D^*K^+$ mode with $D^* \to D\gamma$ is performed in a similar way. The photon candidate is required to have an energy greater than 100 MeV, and the mass difference requirement is $\Delta M < 152\ {\rm MeV}/c^2$. Because of the larger number of background sources for this mode, the treatment of background differs. The $B\bar{B}$ background is subdivided into events with combinatorial D, studied using a generic MC sample; and those with real neutral D mesons, for which a dedicated simulation of each component is performed. The fractions of background components are obtained from an unbinned 4D fit of the distribution of variables $M_{\rm bc}$, ΔE, $\cos\theta_{\rm thr}$, and $\mathcal{F}$. The relative fractions of $B\bar{B}$ backgrounds with a real D^0 (except for $B^{\pm} \to D^*\pi^{\pm}$ and $B^{\pm} \to DK^{\pm}$) are fixed according to their Particle Data Group branching ratios [22] and MC efficiencies. The ΔE and $M_{\rm bc}$ distributions for this mode are shown in Fig. 1(e) and 1(f). The number of events in the signal box is 141, and the signal purity is $(41.7 \pm 3.6)\%$. The continuum background fraction is $(15.8 \pm 1.3)\%$, the fraction of $B\bar{B}$ background with combinatorial D^0 is $(21.3 \pm 3.0)\%$, the contribution of $B^{\pm} \to D^*\pi^{\pm}$, $D^* \to D\gamma$ is $(6.5 \pm 1.2)\%$, and the fraction of the rest of $B\bar{B}$ events with real D^0 is $(14.7 \pm 1.1)\%$.

The Dalitz distributions of $D \to K^0_S\pi^+\pi^-$ decay in the signal box for each of the $B^{\pm} \to DK^{\pm}$ and $B^{\pm} \to D^*K^{\pm}$ processes are shown in Fig. 3.

III. DETERMINATION OF THE $\bar{D}^0 \to K^0_S\pi^+\pi^-$ DECAY AMPLITUDE

As in our previous analysis [12], the $\bar{D}^0 \to K^0_S\pi^+\pi^-$ decay amplitude is represented using the isobar model. The list of resonances is also the same, the only difference being the free parameters (mass and width) of the $K^*(892)^{\pm}$ and $\rho(770)$ states. A modified amplitude, where the scalar $\pi\pi$ component is described using the K-matrix approach [23], is used in the estimation of the systematic error.

The amplitude f for the $\bar{D}^0 \to K^0_S\pi^+\pi^-$ decay is described by a coherent sum of N two-body decay amplitudes and one nonresonant decay amplitude,

$$f(m^2_+, m^2_-) = \sum_{j=1}^{N} a_j e^{i\xi_j} \mathcal{A}_j(m^2_+, m^2_-) + a_{\rm NR} e^{i\xi_{\rm NR}}, \quad (2)$$

where $\mathcal{A}_j(m^2_+, m^2_-)$ is the matrix element, a_j and ξ_j are the amplitude and phase of the matrix element, respectively, of the jth resonance, and $a_{\rm NR}$ and $\xi_{\rm NR}$ are the amplitude and phase, respectively, of the nonresonant

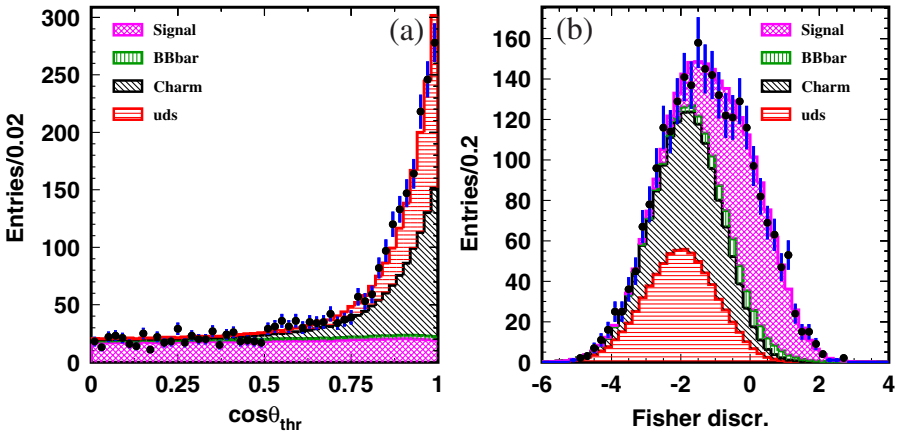

FIG. 2 (color online). $\cos\theta_{\rm thr}$ and $\mathcal{F}$ distributions for the $B^+ \to DK^+$ event sample. Points with error bars show the data with $M_{\rm bc} > 5.27$ MeV/c^2 and $|\Delta E| < 30$ MeV requirements, and the histograms are fitted contributions due to signal, $B\bar{B}$, charm, and (u, d, s) backgrounds.

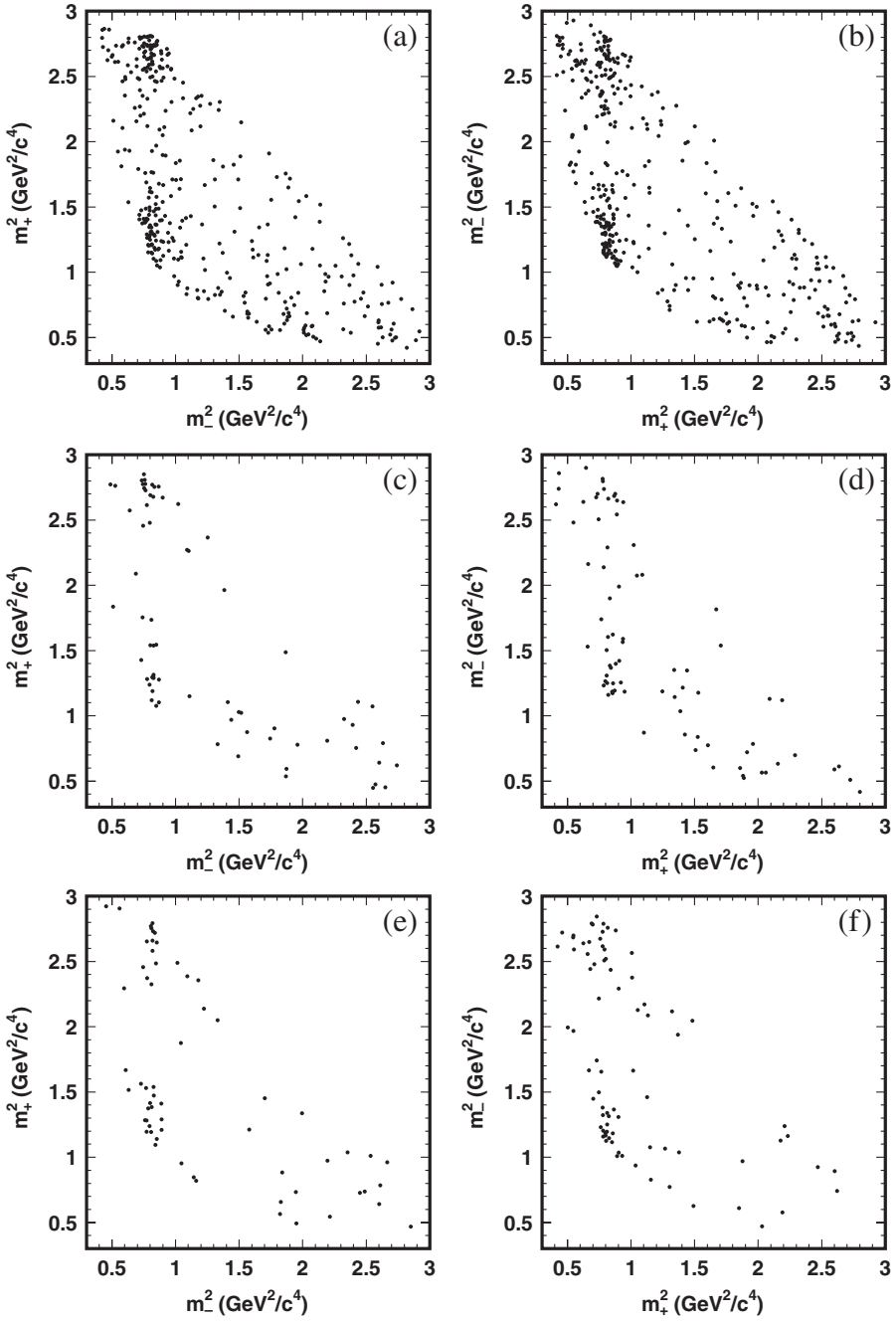

FIG. 3. Dalitz distributions of $D \to K_S^0\pi^+\pi^-$ decays from selected $B^\pm \to DK^\pm$ (a),(b), $B^\pm \to D^*K^\pm$ with $D^* \to D\pi^0$ (c),(d), and $B^\pm \to D^*K^\pm$ with $D^* \to D\gamma$ (e),(f), shown separately for B^- (left) and B^+ (right) tags.

component. The description of the matrix elements follows Ref. [24]. We use a set of 18 two-body amplitudes. These include five Cabibbo-allowed amplitudes: $K^*(892)^+\pi^-$, $K^*(1410)^+\pi^-$, $K_0^*(1430)^+\pi^-$, $K_2^*(1430)^+\pi^-$, and $K^*(1680)^+\pi^-$; their doubly Cabibbo-suppressed partners; and eight amplitudes with K_S^0 and a $\pi\pi$ resonance: $K_S^0\rho$, $K_S^0\omega$, $K_S^0 f_0(980)$, $K_S^0 f_2(1270)$, $K_S^0 f_0(1370)$, $K_S^0\rho(1450)$, $K_S^0\sigma_1$, and $K_S^0\sigma_2$.

We use an unbinned maximum likelihood technique to fit the Dalitz plot distribution to the model described by Eq. (2) with efficiency variation, background contributions, and finite momentum resolution taken into account. The free parameters of the minimization are the amplitudes a_j and phases ξ_j of the resonances, the amplitude $a_{\rm NR}$ and phase $\xi_{\rm NR}$ of the nonresonant component, and the masses and widths of the σ_1 and σ_2 scalars. We also allow the masses and widths of the $K^*(892)^+$ and $\rho(770)$ states to float.

The procedures for determining the background density, the efficiency, and the resolution are the same as in the

previous analyses [12,14]. The background density for $\bar{D}^0 \to K^0_S\pi^+\pi^-$ events is extracted from ΔM sidebands. The shape of the efficiency over the Dalitz plot, as well as the invariant mass resolution, is extracted from the signal Monte Carlo simulation.

The fit results are given in Table I. The fit fraction for each mode is defined as the ratio of the integrals of the squared absolute value of the amplitude for that mode and the squared absolute value of the total amplitude. The fit fractions do not sum up to unity due to interference effects. The parameters obtained for the σ_1 resonance [$M_{\sigma_1} = (522 \pm 6)$ MeV/c^2, $\Gamma_{\sigma_1} = (453 \pm 10)$ MeV/c^2] are similar to those found by other experiments [25,26]. The second scalar term σ_2 is introduced to account for a structure observed at $m^2_{\pi\pi} \sim 1.1$ GeV$^2/c^4$: the fit finds a small but significant contribution with $M_{\sigma_2} = (1033 \pm 7)$ MeV/c^2, $\Gamma_{\sigma_2} = (88 \pm 7)$ MeV/c^2. Allowing the parameters of the dominant $K^*(892)^+$ and $\rho(770)$ resonances to float results in a significant improvement in the fit quality. We obtain $M(K^*(892)) = (893.7 \pm 0.1)$ MeV/c^2, $\Gamma(K^*(892)) = (48.4 \pm 0.2)$ MeV/c^2, $M(\rho) = (771.7 \pm 0.7)$ MeV/c^2, and $\Gamma(\rho) = (136.0 \pm 1.3)$ MeV/c^2.

We perform a χ^2 test using 54×54 bins in the region bounded by $m^2_\pm = 0.3$ and 3.0 GeV$^2/c^4$. The bins with an expected population of less than 50 events are combined with adjacent ones. We find $\chi^2/ndf = 2.35$ for 1065 degrees of freedom (ndf), which is large. We find that the main features of the Dalitz plot are well-reproduced, with some significant but numerically small discrepancies at peaks and dips of the distribution. In our final results we include a conservative contribution to the systematic error due to uncertainties in the $\bar{D}^0$ decay model.

TABLE I. Fit results for $\bar{D}^0 \to K^0_S\pi^+\pi^-$ decay. Errors are statistical only.

Intermediate state	Amplitude	Phase (°)	Fit fraction (%)
$K_S\sigma_1$	1.56 ± 0.06	214 ± 3	11.0 ± 0.7
$K_S\rho^0$	1.0 (fixed)	0 (fixed)	21.2 ± 0.5
$K_S\omega$	0.0343 ± 0.0008	112.0 ± 1.3	0.526 ± 0.014
$K_Sf_0(980)$	0.385 ± 0.006	207.3 ± 2.3	4.72 ± 0.05
$K_S\sigma_2$	0.20 ± 0.02	212 ± 12	0.54 ± 0.10
$K_Sf_2(1270)$	1.44 ± 0.04	342.9 ± 1.7	1.82 ± 0.05
$K_Sf_0(1370)$	1.56 ± 0.12	110 ± 4	1.9 ± 0.3
$K_S\rho^0(1450)$	0.49 ± 0.08	64 ± 11	0.11 ± 0.04
$K^*(892)^+\pi^-$	1.638 ± 0.010	133.2 ± 0.4	62.9 ± 0.8
$K^*(892)^-\pi^+$	0.149 ± 0.004	325.4 ± 1.3	0.526 ± 0.016
$K^*(1410)^+\pi^-$	0.65 ± 0.05	120 ± 4	0.49 ± 0.07
$K^*(1410)^-\pi^+$	0.42 ± 0.04	253 ± 5	0.21 ± 0.03
$K^*_0(1430)^+\pi^-$	2.21 ± 0.04	358.9 ± 1.1	7.93 ± 0.09
$K^*_0(1430)^-\pi^+$	0.36 ± 0.03	87 ± 4	0.22 ± 0.04
$K^*_2(1430)^+\pi^-$	0.89 ± 0.03	314.8 ± 1.1	1.40 ± 0.06
$K^*_2(1430)^-\pi^+$	0.23 ± 0.02	275 ± 6	0.093 ± 0.014
$K^*(1680)^+\pi^-$	0.88 ± 0.27	82 ± 17	0.06 ± 0.04
$K^*(1680)^-\pi^+$	2.1 ± 0.2	130 ± 6	0.30 ± 0.07
Nonresonant	2.7 ± 0.3	160 ± 5	5.0 ± 1.0

IV. DALITZ PLOT ANALYSIS OF $B^+ \to D^{(*)}K^+$ DECAYS

As in our previous analysis [12] and in analyses carried out by the *BABAR* Collaboration [15,16], we fit the Dalitz distributions of the B^+ and B^- samples separately, using Cartesian parameters $x_\pm = r_\pm\cos(\pm\phi_3 + \delta)$ and $y_\pm = r_\pm\sin(\pm\phi_3 + \delta)$, where the indices "+" and "−" correspond to B^+ and B^- decays, respectively. In this approach the amplitude ratios (r_+ and r_-) are not constrained to be equal for the B^+ and B^- samples. Confidence intervals in r, ϕ_3, and δ are then obtained from the $(x_\pm, y_\pm)$ using a frequentist technique. The advantage of this approach is low bias and simple distributions of the fitted parameters, at the price of fitting in a space with higher dimensionality (x_+, y_+, x_-, y_-) than that of the physical parameters (r, ϕ_3, δ); see Sec. V.

Following the procedure described in Sec. II, background events for the $B^\pm \to DK^\pm$ and $B^\pm \to D^*K^\pm$, $D^* \to D\pi^0$ modes are classified into four components: $e^+e^- \to q\bar{q}$ (where $q = u, d, s$), charm, $B\bar{B}$ (except for $B^\pm \to D^{(*)}\pi^\pm$), and $B^\pm \to D^{(*)}\pi^\pm$ background. This is a refinement of the previous analysis, where three background components were used, without separation of the continuum background into (u, d, s) and charm. In the case of the $B^\pm \to D^*K^\pm$ mode with $D^* \to D\gamma$, the $B\bar{B}$ background is divided into events with combinatorial D and seven types of events with real D mesons (including modes with a neutral or charged B meson decaying to $D^{(*)}$ and a K, π, or ρ meson).

The distributions of each of the background components are assumed to be factorized into products of a Dalitz plot distribution (m^2_+, m^2_-), and distributions in $(M_{\rm bc}, \Delta E)$, and $(\cos\theta_{\rm thr}, \mathcal{F})$. The shapes of these distributions are extracted from MC simulation. The six-dimensional probability density function (PDF) used for the fit is thus expressed as

$$p = \sum_i p_i(m^2_+, m^2_-)\, p_i(M_{\rm bc}, \Delta E)\, p_i(\cos\theta_{\rm thr}, \mathcal{F}), \qquad (3)$$

where the index i runs over all background contributions and signal. The distributions $p_i(M_{\rm bc}, \Delta E)$ and $p_i(\cos\theta_{\rm thr}, \mathcal{F})$ are parameterized functions. The parameterization of $p_i(M_{\rm bc}, \Delta E)$ differs for different components: sums of two two-dimensional Gaussian distributions with correlations for signal and $B^+ \to D^{(*)}K^+$; products of the empirical shape proposed by the ARGUS Collaboration in $M_{\rm bc}$ [27] and a linear function in ΔE for $q\bar{q}$, charm, and $B\bar{B}$ components. In addition, the parameterization for $B\bar{B}$ background includes a product of a Gaussian peak in $M_{\rm bc}$ and a sum of exponential and Gaussian distributions in ΔE. We represent $p_i(\cos\theta_{\rm thr}, \mathcal{F})$ as the product of two terms: (i) the exponential of a fourth-degree polynomial in $\cos\theta_{\rm thr}$, and (ii) a sum of bifurcated Gaussian distributions

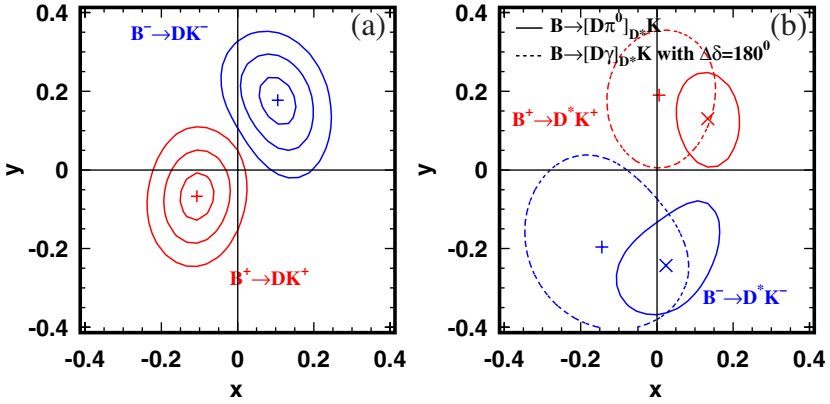

FIG. 4 (color online). Results of signal fits with free parameters $x = r\cos\theta$ and $y = r\sin\theta$ for $B^+ \to DK^+$ (a) and $B^+ \to D^*K^+$ (b) samples, separately for B^- and B^+ data. Contours indicate 1, 2, and 3 (for $B^\pm \to DK^\pm$) and 1 standard deviation regions (for $B^\pm \to D^*K^\pm$) obtained in the maximum likelihood fit. For the $B^\pm \to D^*K^\pm$, $D^* \to D\gamma$ mode, the sign of $x_\pm$ and $y_\pm$ is swapped to account for the relative strong phase difference of 180° with respect to the $B^\pm \to D^*K^\pm$, $D^* \to D\pi^0$ sample.

in $\mathcal{F}$, where the mean and the various widths have a polynomial dependence on $\cos\theta_{\rm thr}$. The function $p_i(m_+^2, m_-^2)$ is represented by Gaussian smoothing of the MC data.

At the first stage of the analysis (as described in Sec. II) we determine the relative fractions of each background component by performing an unbinned maximum likelihood fit to the experimental data in $M_{\rm bc}$ and ΔE ($M_{\rm bc}$, ΔE, $\cos\theta_{\rm thr}$, and $\mathcal{F}$ for $B^\pm \to D^*K^\pm$, $D^* \to D\gamma$). The free parameters in the fit are the fractions of continuum, $B\bar{B}$, and $B^\pm \to D^{(*)}\pi^\pm$ events. The relative fractions of the (u, d, s) and charm components of the continuum background and the relative fractions of $B\bar{B}$ backgrounds with real D^0 for the $B^\pm \to D^*K^\pm$, $D^* \to D\gamma$ mode are fixed from the MC simulation.

At the second stage, separate Dalitz distributions are formed for the B^+ and B^- samples with the signal requirement for $M_{\rm bc}$ and ΔE ($M_{\rm bc} > 5.27$ GeV/c^2, $|\Delta E| < 30$ MeV) and no requirements for $\cos\theta_{\rm thr}$ and $\mathcal{F}$. In each case, a fit with free parameters x and y is performed with the unbinned maximum likelihood technique, using variables m_+^2, m_-^2, $M_{\rm bc}$, ΔE, $\cos\theta_{\rm thr}$, and $\mathcal{F}$; only the first four variables were used in the previous analysis [12]. Possible deviations from the factorization assumption for the background distribution and disagreements between MC and experimental background densities are treated in the systematic error. The efficiency variation as a function of the Dalitz plot variables is obtained from signal MC simulation and is taken into account in the likelihood function.

To test the consistency of the fit, the same procedure as used for the $B^+ \to D^{(*)}K^+$ signal was applied to the $B^+ \to D^{(*)}\pi^+$ control samples. For the $B^\pm \to D\pi^\pm$ and $B^\pm \to D^*\pi^\pm$ ($D^* \to D\pi^0$) modes, the results are consistent with the expected value $r \sim 0.01$ for the amplitude ratio. For $B^\pm \to D^*\pi^\pm$ ($D^* \to D\gamma$), we find $r = 0.05 \pm 0.02$, which is larger than the expected value by 2 standard deviations. Inspection of the Dalitz distributions shows visible differences between B^+ and B^- data in this mode: we interpret the large value of r as a statistical fluctuation.

The results of the separate B^+ and B^- data fits are shown in Fig. 4. The values of the fit parameters $x_\pm$ and $y_\pm$ are listed in Table II. As expected, the values of $x_\pm$ and $y_\pm$ for the $D^* \to D\gamma$ and $D^* \to D\pi^0$ modes from $B^\pm \to D^*K^\pm$ agree within the statistical errors after reversing the signs in one of the modes.

V. EVALUATION OF THE STATISTICAL ERRORS

We use a frequentist technique to evaluate the statistical significance of the measurements. The procedure is iden-

TABLE II. Results of the signal fits in parameters (x, y). The first error is statistical, and the second is experimental systematic error. Statistical correlation coefficients between x and y are also shown. Model uncertainty is not included.

Parameter	$B^+ \to DK^+$	$B^+ \to D^*K^+$, $D^* \to D\pi^0$	$B^+ \to D^*K^+$, $D^* \to D\gamma$
x_-	$+0.105 \pm 0.047 \pm 0.011$	$+0.024 \pm 0.140 \pm 0.018$	$+0.144 \pm 0.208 \pm 0.025$
y_-	$+0.177 \pm 0.060 \pm 0.018$	$-0.243 \pm 0.137 \pm 0.022$	$+0.196 \pm 0.215 \pm 0.037$
$x_- - y_-$ correlation	-0.289	$+0.440$	-0.207
x_+	$-0.107 \pm 0.043 \pm 0.011$	$+0.133 \pm 0.083 \pm 0.018$	$-0.006 \pm 0.147 \pm 0.025$
y_+	$-0.067 \pm 0.059 \pm 0.018$	$+0.130 \pm 0.120 \pm 0.022$	$-0.190 \pm 0.177 \pm 0.037$
$x_+ - y_+$ correlation	$+0.110$	-0.101	$+0.080$

tical to that in our previous analysis [12]. This method requires knowledge of the PDF of the reconstructed parameters x and y as a function of the true parameters $\bar{x}$ and $\bar{y}$. To obtain this PDF, we use a simplified MC simulation of the experiment which incorporates a maximum likelihood fit with the same efficiencies, resolution, and backgrounds as used in the fit to the experimental data.

Figure 5 shows the projections of the three-dimensional confidence regions onto the (r, ϕ_3) and (ϕ_3, δ) planes for the $B^\pm \to DK^\pm$ and $B^\pm \to D^*K^\pm$ modes. In the results for the $B^\pm \to D^*K^\pm$ mode, we combine both $D^* \to D\pi^0$ and $D^* \to D\gamma$ final states, taking into account the relative strong phase of 180° between them by swapping the sign of the x and y parameters for the $D^* \to D\gamma$ mode. We show the 20%, 74%, and 97% confidence level regions, which correspond to 1, 2, and 3 standard deviations for a three-dimensional Gaussian distribution. The values of the parameters r, ϕ_3, and δ obtained for the $B^\pm \to DK^\pm$ and $B^\pm \to D^*K^\pm$ modes separately are given in Table III. The values of ϕ_3 in these modes agree within the statistical errors. In general, r and δ may differ: our results for r are similar for the two modes, while the δ values are distinct.

Note that our statistical procedure gives three-dimensional confidence level regions. The coverage for the set of three parameters (r, ϕ_3, δ) is exact. One-dimensional intervals are obtained by projecting the three-dimensional regions onto each of the parameter axes: exact coverage for this procedure is ensured only in the case of Gaussian errors. In our case, Gaussian behavior of the errors is reached when $\sigma(r) \ll r$, and undercoverage (effectively, underestimation of statistical errors) occurs if $\sigma(r) \sim r$. The amount of undercoverage depends on the true value $\bar{r}$: errors are underestimated by a factor ranging from 1.4 for $\bar{r} = 0$ to 1.03 for $\bar{r}$ equal to the measured value.

TABLE III. *CP* fit results. The first error is statistical, the second is experimental systematic, and the third is the model uncertainty.

Parameter	$B^+ \to DK^+$ mode	$B^+ \to D^*K^+$ mode
ϕ_3	$(80.8^{+13.1}_{-14.8} \pm 5.0 \pm 8.9)°$	$(73.9^{+18.9}_{-20.2} \pm 4.2 \pm 8.9)°$
r	$0.161^{+0.040}_{-0.038} \pm 0.011^{+0.050}_{-0.010}$	$0.196^{+0.073}_{-0.072} \pm 0.013^{+0.062}_{-0.012}$
δ	$(137.4^{+13.0}_{-15.7} \pm 4.0 \pm 22.9)°$	$(341.7^{+18.6}_{-20.9} \pm 3.2 \pm 22.9)°$

VI. ESTIMATION OF SYSTEMATIC ERROR

Experimental systematic errors come from uncertainty in the knowledge of the distributions used in the fit [i.e. Dalitz plot distributions of the background components, and the $(M_{\rm bc}, \Delta E)$ and $(\cos\theta_{\rm thr}, \mathcal{F})$ distributions of the backgrounds and signal], fractions of different background components, and the distribution of the efficiency across the Dalitz plot. Uncertainties in background shapes are

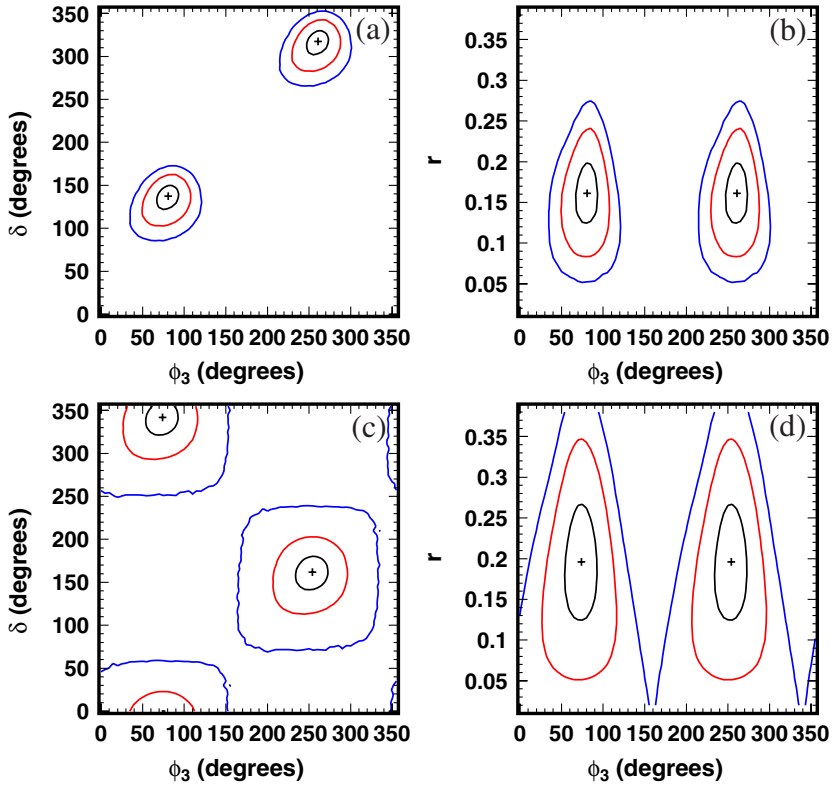

FIG. 5 (color online). Projections of confidence regions for the $B^+ \to DK^+$ (a),(b) and $B^+ \to D^*K^+$ (c),(d) mode onto the (r, ϕ_3) and (ϕ_3, δ) planes. Contours indicate projections of 1, 2, and 3 standard deviation regions.

estimated by using alternative distributions in the fit (extracted from experimental data where possible). Uncertainties in the background fractions are obtained by varying each fraction within its error. Possible correlations in the distributions for background components that are not described by the formula (3) are estimated by using independent background distributions in the bins of $M_{\rm bc}$, ΔE, $\cos\theta_{\rm thr}$, and $\mathcal{F}$ variables.

In the case of $B^\pm \to D^* K^\pm$, $D^* \to D\gamma$ decay, an additional uncertainty arises from the significant cross feed from the $B^\pm \to D^* K^\pm$, $D^* \to D\pi^0$ mode. The baseline $D^* \to D\gamma$ fit uses x and y values obtained from the $B^\pm \to D^* K^\pm$, $D^* \to D\pi^0$ fit for modeling the $D^* \to D\pi^0$ cross feed; to estimate the systematic uncertainty, we vary x and y within their errors and also take $x = y = 0$. As an additional check, we apply a $D^* \to D\pi^0$ veto to the $B^\pm \to D^* K^\pm$, $D^* \to D\gamma$ sample: the results of this fit are consistent with the baseline results within statistical errors.

The procedure for estimating the uncertainty due to the detection efficiency is different from that in the previous analysis [12]: here we use an alternative efficiency shape obtained by MC simulation from the parameterized track finding efficiency (extracted from experimental data) as a function of transverse momentum and polar angle θ.

Compared to our previous analysis [12], an additional source of systematic error exists due to the use of $\cos\theta_{\rm thr}$ and $\mathcal{F}$ variables in the fit. However, the use of these variables increases the effective signal-to-background ratio, so the total systematic error is comparable.

Systematic errors in the physical parameters r, ϕ_3, and δ are calculated from the systematic errors on the fitted parameters (x, y). Values (x, y) are generated according to Gaussian distributions with standard deviations equal to the corresponding total systematic errors; parameters r, ϕ_3, and δ are then obtained for each (x, y) set, and the root-mean-square deviations of the resulting values are calculated. We perform this procedure in two ways: without correlation of (x, y) biases for B^+ and B^-, and with 100% correlation between them. The larger root-mean-square deviation of the two options is chosen as the systematic error. The systematic errors in the x and y variables are shown in Table II.

The model used for the $\bar{D}^0 \to K^0_S \pi^+ \pi^-$ decay amplitude is one of the main sources of error for our analysis: we list this contribution separately. The model uncertainty splits into two contributions: one due to imperfect description of the observable D^0 Dalitz plot distribution, and one due to uncertainty of the phase of the complex amplitude f, which is based purely on the model assumptions and appears even in the case of a perfect description of the experimental $\bar{D}^0$ data. To estimate the former contribution, we use model variations that give a similar $\bar{D}^0 \to K^0_S \pi^+ \pi^-$ fit quality to that of the default model. For the latter contribution, we take the complex phase of $f(m^2_+, m^2_-)$ from models with a reduced number of resonances as in the previous analysis [12] while keeping the absolute value of the amplitude the same as in the default model. The total model uncertainty $\Delta\phi_3 = 8.9°$ is dominated by the uncertainty due to the complex phase. Note that the model errors on r are highly asymmetric. While an imperfect description of the D^0 density can lead to a bias in both directions, a wrong complex phase introduces a bias only to lower values.

Our estimate of the model uncertainty can be considered conservative. When the various S-wave terms—the most theoretically controversial part of the model—are replaced by a K-matrix amplitude [23], the change in ϕ_3 from the baseline fit does not exceed 2°. However, we retain our default 8.9° uncertainty as the K matrix describes only part of the amplitude.

Using a different approach, it is possible to remove the current model uncertainty, exploiting constraints on the complex phase in the $\bar{D}^0 \to K^0_S \pi^+ \pi^-$ amplitude that can be obtained experimentally from the analysis of $\psi(3770) \to D^0 \bar{D}^0$ decays. Such a measurement was recently performed by CLEO [28]. The results show good agreement with the isobar model; however, a quantitative estimate of the model uncertainty for a model-dependent fit is hard to obtain from these data. Instead, a model-independent analysis [7,29,30] involving a binned fit of the $\bar{D}^0 \to K^0_S \pi^+ \pi^-$ Dalitz distribution is possible. The model error in this analysis will be replaced by a statistical error of about 1°–2° due to the finite $\psi(3770) \to D^0 \bar{D}^0$ sample, while the statistical error associated with the B data sample should increase by 10%–20% due to the binned fit procedure. At the current level of precision, this will not result in a significant improvement in the precision of ϕ_3, but future analyses with larger samples of B decays should benefit from the model-independent technique.

VII. COMBINED ϕ_3 MEASUREMENT

The two event samples $B^+ \to DK^+$ and $B^+ \to D^* K^+$ are combined in order to improve the sensitivity to ϕ_3. The confidence levels for the combination of the two modes are obtained using the same frequentist technique as for the single mode, with the PDF of the two measurements being the product of the probability densities for the individual modes. Confidence intervals for the combined measurement together with systematic and model errors are shown in Table IV. The statistical confidence level of CP violation is $1 - \text{C.L.} = 1.5 \times 10^{-4}$, or 3.8 standard deviations. With the systematic and model errors taken into account, CP conservation is ruled out at the confidence level 5×10^{-4}, or 3.5 standard deviations. The systematic errors are assumed to be uncorrelated in this calculation; the resulting estimate is conservative, as most of the systematic biases

TABLE IV. Results of the combination of the $B^+ \to DK^+$ and $B^+ \to D^*K^+$ modes.

Parameter	1σ interval	2σ interval	Systematic error	Model uncertainty
ϕ_3	$(78.4^{+10.8}_{-11.6})^\circ$	$54.2^\circ < \phi_3 < 100.5^\circ$	3.6°	8.9°
r_{DK}	$0.160^{+0.040}_{-0.038}$	$0.084 < r_{DK} < 0.239$	0.011	$+0.050 - 0.010$
r_{D^*K}	$0.196^{+0.072}_{-0.069}$	$0.061 < r_{D^*K} < 0.271$	0.012	$+0.062 - 0.012$
δ_{DK}	$(136.7^{+13.0}_{-15.8})^\circ$	$102.2^\circ < \delta_{DK} < 162.3^\circ$	4.0°	22.9°
δ_{D^*K}	$(341.9^{+18.0}_{-19.6})^\circ$	$296.5^\circ < \delta_{D^*K} < 382.7^\circ$	3.0°	22.9°

are correlated between B^+ and B^- samples and thus do not introduce CP violation.

VIII. CONCLUSION

We report the results of a measurement of the unitarity triangle angle ϕ_3, using a method based on Dalitz plot analysis of $\bar{D}^0 \to K^0_S\pi^+\pi^-$ decay in the process $B^+ \to D^{(*)}K^+$. A new measurement of ϕ_3 using this technique was performed based on 605 fb^{-1} of data collected by the Belle detector: 70% larger than the previous sample [12]. The statistical sensitivity of the measurement has also been improved by modifications to the event selection and fit procedure, and by adding the sample with D^* decaying to the $D\gamma$ final state.

From the combination of $B^+ \to DK^+$ and $B^+ \to D^*K^+$ modes, we obtain the value $\phi_3 = 78.4^\circ(\text{stat}) \pm 3.6^\circ(\text{syst}) \pm 8.9^\circ(\text{model}) - 11.6^\circ + 10.8^\circ$; of two possible solutions we have chosen the one with $0 < \phi_3 < 180^\circ$. We also obtain values of the amplitude ratios $r_{DK} = 0.160^{+0.040}_{-0.038}(\text{stat}) \pm 0.011(\text{syst})^{+0.050}_{-0.010}(\text{model})$ and $r_{D^*K} = 0.196^{+0.072}_{-0.069}(\text{stat}) \pm 0.012(\text{syst})^{+0.062}_{-0.012}(\text{model})$. The CP conservation in the combined measurement is ruled out at the confidence level 5×10^{-4}, or 3.5 standard deviations.

The statistical precision of the ϕ_3 measurement is already comparable to the estimated model uncertainty. However, it is possible to eliminate this model uncertainty using constraints on the $\bar{D}^0 \to K^0_S\pi^+\pi^-$ decay amplitude obtained by the CLEO Collaboration in the analysis of $\psi(3770) \to D^0\bar{D}^0$ decays [28–30]. The statistical errors in the proposed binned fit procedure are 10%–20% larger, but the model uncertainty is replaced by a small (1°–2°) statistical error due to the finite $\psi(3770) \to D^0\bar{D}^0$ sample. This should result in an improvement of the ϕ_3 precision in future high-statistics analyses.

ACKNOWLEDGMENTS

We thank the KEKB group for the excellent operation of the accelerator, the KEK cryogenics group for the efficient operation of the solenoid, and the KEK computer group and the National Institute of Informatics for valuable computing and SINET3 network support. We acknowledge support from the Ministry of Education, Culture, Sports, Science, and Technology (MEXT) of Japan, the Japan Society for the Promotion of Science (JSPS), and the Tau-Lepton Physics Research Center of Nagoya University; the Australian Research Council and the Australian Department of Industry, Innovation, Science and Research; the National Natural Science Foundation of China under Contracts No. 10575109, No. 10775142, No. 10875115, and No. 10825524; the Ministry of Education, Youth and Sports of the Czech Republic under Contract No. LA10033; the Department of Science and Technology of India; the BK21 and WCU program of the Ministry Education Science and Technology, National Research Foundation of Korea, and NSDC of the Korea Institute of Science and Technology Information; the Polish Ministry of Science and Higher Education; the Ministry of Education and Science of the Russian Federation and the Russian Federal Agency for Atomic Energy; the Slovenian Research Agency; the Swiss National Science Foundation; the National Science Council and the Ministry of Education of Taiwan; and the U.S. Department of Energy. This work is supported by a Grant-in-Aid from MEXT for Science Research in a Priority Area (''New Development of Flavor Physics'') and from JSPS for Creative Scientific Research (''Evolution of Tau-lepton Physics'').

[1] M. Kobayashi and T. Maskawa, Prog. Theor. Phys. **49**, 652 (1973); N. Cabibbo, Phys. Rev. Lett. **10**, 531 (1963).
[2] M. Gronau and D. London, Phys. Lett. B **253**, 483 (1991); M. Gronau and D. Wyler, Phys. Lett. B **265**, 172 (1991).
[3] I. Dunietz, Phys. Lett. B **270**, 75 (1991).
[4] D. Atwood, G. Eilam, M. Gronau, and A. Soni, Phys. Lett. B **341**, 372 (1995).
[5] D. Atwood, I. Dunietz, and A. Soni, Phys. Rev. Lett. **78**, 3257 (1997); Phys. Rev. D **63**, 036005 (2001).
[6] I. I. Bigi and A. I. Sanda, Phys. Lett. B **211**, 213 (1988);

A. B. Carter and A. I. Sanda, Phys. Rev. Lett. **45**, 952 (1980).
[7] A. Giri, Yu. Grossman, A. Soffer, and J. Zupan, Phys. Rev. D **68**, 054018 (2003).
[8] A. Bondar, in Proceedings of BINP Special Analysis Meeting on Dalitz Analysis, 2002 (unpublished).
[9] L. Wolfenstein, Phys. Rev. Lett. **51**, 1945 (1983).
[10] A. J. Schwartz (HFAG charm group), arXiv:0911.1464.
[11] Y. Grossman, A. Soffer, and J. Zupan, Phys. Rev. D **72**, 031501 (2005).
[12] A. Poluektov *et al.* (Belle Collaboration), Phys. Rev. D **73**, 112009 (2006).
[13] K. Abe *et al.* (Belle Collaboration), arXiv:hep-ex/0308043.
[14] A. Poluektov *et al.* (Belle Collaboration), Phys. Rev. D **70**, 072003 (2004).
[15] B. Aubert *et al.* (*BABAR* Collaboration), Phys. Rev. Lett. **95**, 121802 (2005).
[16] B. Aubert *et al.* (*BABAR* Collaboration), Phys. Rev. D **78**, 034023 (2008).
[17] B. Aubert *et al.* (*BABAR* Collaboration), Phys. Rev. Lett. **99**, 251801 (2007).
[18] A. Abashian *et al.* (Belle Collaboration), Nucl. Instrum. Methods Phys. Res., Sect. A **479**, 117 (2002).
[19] Y. Ushiroda *et al.* (Belle SVD2 Group), Nucl. Instrum. Methods Phys. Res., Sect. A **511**, 6 (2003).
[20] A. Bondar and T. Gershon, Phys. Rev. D **70**, 091503 (2004).
[21] D. M. Asner *et al.* (CLEO Collaboration), Phys. Rev. D **53**, 1039 (1996).
[22] C. Amsler *et al.* (Particle Data Group), Phys. Lett. B **667**, 1 (2008).
[23] V. V. Anisovich and A. V. Sarantsev, Eur. Phys. J. A **16**, 229 (2003).
[24] S. Kopp *et al.* (CLEO Collaboration), Phys. Rev. D **63**, 092001 (2001).
[25] H. Muramatsu *et al.* (CLEO Collaboration), Phys. Rev. Lett. **89**, 251802 (2002); **90**, 059901(E) (2003).
[26] E. M. Aitala *et al.* (E791 Collaboration), Phys. Rev. Lett. **86**, 770 (2001).
[27] H. Albrecht *et al.* (ARGUS Collaboration), Phys. Lett. B **241**, 278 (1990).
[28] R. A. Briere *et al.* (CLEO Collaboration), Phys. Rev. D **80**, 032002 (2009).
[29] A. Bondar, A. Poluektov, Eur. Phys. J. C **47**, 347 (2006).
[30] A. Bondar, A. Poluektov, Eur. Phys. J. C **55**, 51 (2008).